Research Article

Jinxin He, Debo Chen*, Ye Zhan, Xiaoyu Ren, and Qingyi Li

A retrieval model of surface geochemistry composition based on remotely sensed data

https://doi.org/10.1515/geo-2022-0514
received May 21, 2022; accepted July 02, 2023

Abstract: The geochemical sampling work in the difficult and dangerous areas is very hard; hence, it can be greatly improved by combining with the remotely sensed data. Thus, a retrieval model is proposed by Kernel Principal Component Analysis and Artificial Bee Colony (ABC) optimized Support Vector Machine (SVM) models based on Landsat 8 remotely sensed data and the geochemical data in the study area. The analysis results show that the geochemical data delineate the areas with relatively enriched elements, but indicate the low-abnormal ore (chemical) points, and the anomalies delineated by the inversion data are better for this purpose, for better indication. At the same time, the distribution and intensity of the corresponding abnormal areas found that the abnormal areas delineated by the inversion data basically contain the abnormal areas delineated by the original data, and the anomalies located at the ore spots are obviously enhanced; it shows that the SVM model of ABC Optimization can establish the relation between geochemistry data and remote sensing data, can supply the original data effectively, and can also provide the direction for the next prospecting work.

Keywords: Landsat 8, geochemistry, kernel principal component analysis, artificial bee colony, support vector machine

1 Introduction

The collection of geochemical data is very labor-intensive and material-intensive, especially in some areas where the natural environment is harsh. In response to this problem, remote sensing geochemistry [1] combines the advantages of geochemistry with remote sensing technology, in terms of both the spatial and the temporal advantages of remote sensing data acquisition and in terms of the chemical element distribution [2]. Previous studies have shown that features in the remote sensing spectrum, such as absorption valleys, are related to specific units in the corresponding substances, such as hydroxyl and manganese ions [3], but are also affected by the element contents [4]. Therefore, it is theoretically possible to retrieve the geochemistry data from the remote sensing data.

For example, Aronoff and Goodfellow [5] and Eliason et al. [6] added the image factor to their geochemical study as early as the 1980s and take the Lake Kuayat region in Canada as an example combining remote sensing image and stream sediment data in this area; the prospecting work is carried out using the integrated information, and the result is better than the single method. Zhang [7] studied the remote sensing information, the geochemical information, and the buffer area information of the study area to get comprehensive information and used it to guide the prospecting work and got better results than the single information. Zhao [8] used the least squares method to extract the features of ETM+ remote sensing data, considered the spatial attributes of geochemical data, and established the point-to-point spatial relationship between remote sensing data and geochemical data; finally, a retrieval model is established between the extracted features and the geochemical data by using the limit learning machine model. Pan Cencen used the local correlation maximum approach for spectral data preprocessing and conducted the comparative studies in a series of models, including Partial Least Squares (PLS), Support Vector Machine (SVM), Least Absolute Shrinkage and Selection Operator, Elastic Network, Regularization Random Forest and Ridge Regression Coefficient Screening models, and the results show that the Regularization Random Forest has the best result [9]. Ren et al. used the geochemical data to identify the geologic background of lithological formation; because of the uniqueness of the data, they used genetic algorithms to optimize the neural network, and the experimental results show that the discriminant ability is superior [10]. Li et al. studied lunar surface minerals using PLSR and BP neural networks [11]. Bachri

* **Corresponding author: Debo Chen,** College of Earth Sciences, Jilin University, Changchun, 130061 China, e-mail: 591022245@qq.com
Jinxin He, Xiaoyu Ren, Qingyi Li: College of Earth Sciences, Jilin University, Changchun, 130061 China
Ye Zhan: Aviation University Air Force, Changchun, 130021 China

et al. used SVM for automatic lithology mapping based on remote sensing data [12]. Yunkai et al. chose four methods to preprocess hyperspectral remote sensing data and found that the first-order differential transformation is the best, and the characteristics of data nonlinearity are taken into account; the PLS kernel functions are used to obtain the kernel PLSs, which is better than the traditional multiple regression in the process of geochemical element retrieval [13]. Chengzhao et al. combined Principal Component Analysis with SVM to perform the predictive analysis [14].

Based on the previous studies, there are two main problems in constructing the retrieval model: (1) The strong correlation and non-linear characteristics between the remote sensing bands are usually ignored; (2) the retrieval model is not always efficient. Therefore, Kernel Principal Component Analysis (KPCA) is chosen to extract the remote sensing features, and then, the remote sensing data are located according to the geochemical data coordinates. Finally, the parameters of SVM are optimized by Artificial Bee Colony (ABC) model, and the accuracy is verified according to the actual geochemical data in the study area. The whole flow chart is shown in Figure 1.

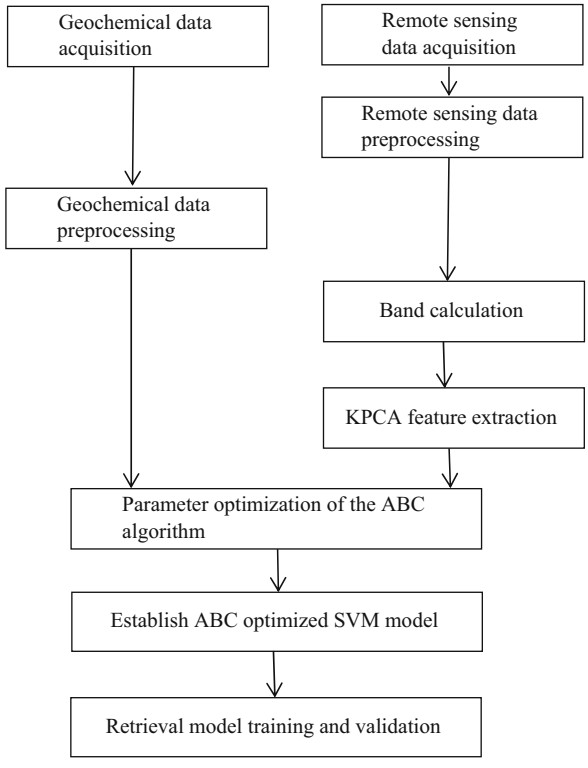

Figure 1: Flowchart of the retrieval model.

2 Geological setting

2.1 Geographic settings

The study area is located between Min County and Li County; there are Zhang County and Wushan County in the middle; roads and national roads are connected, and the transportation is convenient (Figure 2). The study area belongs to the central mountainous area, with a slow inner ridge, interwoven ravines, and a general slope of between 15° and 30°. Vegetation does not develop, but the coverage rate of turf and sand is as high as 80%, the surface coverage is thick, and the bedrock is less exposed, only in the steep and valley floor. This area belongs to a temperate continental climate, with a large temperature difference between the four seasons. The water system is relatively developed, perennial and seasonal rivers crisscross, the central and northern water system into the Tao River, belonging to the Yellow River basin, the southern tributary water system into the Bailong River, belonging to the Jialing River system of the Yangtze River basin.

2.2 Geological settings

The Zhaishang-Mawu exploration area exhibits a distinctive geological structure, with a wide geographical distribution and diverse range of minerals. The identified minerals include iron, copper, lead, zinc, gold, antimony, tungsten, tin, mercury, and other metallic elements. The overall pattern of mineralization can be described as follows: The mineral (chemical) sites are distributed in the NWW direction, and the genesis of mineral distribution transitions from high temperature to medium temperature, and then to low temperature as one moves farther away from the rock body. The formation and distribution of endogenous minerals are strictly controlled by medium acidic intrusive rocks and tectonics from the Indochina and Yanshan periods. These deposits are genetically related to deep-formed granitic magma sources. Different tectonic systems play a significant role in spatially controlling mineralization. The mineralization of lead, zinc, copper, and similar elements occurs at a slight distance from the rock body and is primarily controlled by secondary fractures and fissures. Tungsten and tin ores are mainly found in the contact zone within the rock body, with secondary fractures predominantly oriented along the northeast direction. Molybdenum ores are associated with acidic porphyry bodies and are controlled by secondary fractures oriented north–south. Gold ores predominately occur in the contact zone outside the rock body and are influenced by secondary folds and secondary fractures.

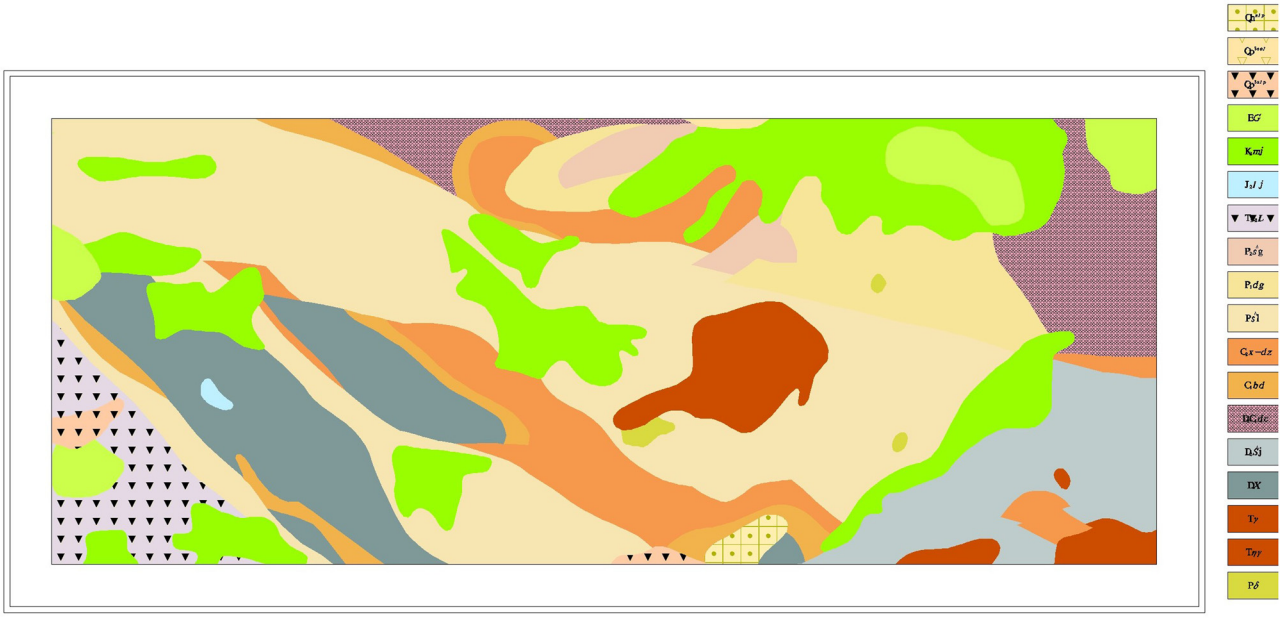

Figure 2: Geological map of the study area.

3 Materials and methods

3.1 Data

3.1.1 Remote sensing data

Some of the parameters of the Landsat 8 OLI remote sensing image, obtained on the USGS website, are shown in Table 1. LC08 indicates the image source satellite Landsat-8, L1TP (Level 1 Precision Terrain) indicates the data Level is L1, and tP indicates that the data have been topographically and geometrically corrected, and 130036 indicates that the area code in the WRS-2 reference system is 130 and the line number is 36, which is Gansu Province; 20160215 represents data acquisition on February 15, 2016, and 20170329 represents data processing on March 2, 2017. The resolution is 30 m.

The files downloaded are in traditional TIFF format, including 11 single-band files, one metadata file, and one BSQ file for quality assessment, which are mainly environmental operating parameters of the sensor, and it can be used to build some spectral analysis files. The metadata files include information such as shot time, solar altitude angle, latitude, and longitude.

Table 1: Landsat 8 OLI remote sensing image characteristics

Central latitude	33.17727
Central longitude	105.32528
Solar azimuth angle	149.64078944
Solar elevation	36.03919797
Data acquisition time	2016-02-15

The acquired remote sensing images are pre-processed, and since the acquired data have been geometrically corrected and topographically corrected, they are directly radiometrically calibrated with atmospheric correction. This step first changes the DN values into radiometric brightness values and then removes atmospheric effects as much as possible by FLASSH atmospheric correction.

3.1.2 Geochemical data

Data were obtained from 1:50,000 aqueous sediment measurements from eight 1:50,000 plots in the Zhaishang–Mawu gold mining area: Meichuan, Puma, Xinshi, Tango, Minxian, Shendu, Locklong, and Mawu, and ten elements were analyzed for Au, Ag, As, Sb, Hg, Cu, Pb, Zn, Mo, and Sn (Table 2). The method of iterative culling is used to cull the distortion points that affect the background and anomaly by pressing $x \pm 3\,\delta$, the sample number (N), average value ($\bar{X}$), standard deviation (δ), variation coefficient (C_v), anomaly area (S), global concentration coefficient (Kk), and superposition strength (D) of the whole area, and each geological unit are calculated, respectively. There are AU, Hg, PB, AG, As, W, and SB in the highly differentiated elements ($C_v\% \geq 75$) in the stream sediments, which indicates that they are highly unevenly distributed in the strata and have a high

Table 2: Characteristics of element contents in stream sediments (10^{-9} for AU and Hg and 10^{-6} for other elements)

Element	Stream deposit								West Qin mountains		Superposition value
	Before culling				After elimination				Mean value	Background value	
	$\overline{X}$	C_v	S	Kk	$\overline{X}_0$	C_{v0}	S_0	Kk_0			
Au	3.19	7.30	23.28	2.02	1.22	0.55	0.67	0.77	1.632	1.58	90.897
Hg	120.44	3.87	465.62	3.66	32.37	0.59	18.96	0.98	75.396	32.91	91.373
Cu	22.83	0.72	16.34	1.03	22.59	6.24	5.23	1.02	22.16	22.24	3.157
Pb	27.81	0.91	25.33	1.22	26.72	0.3	8.01	1.17	33.67	22.88	3.291
Zn	83.91	0.44	36.73	1.27	83.2	0.32	26.43	1.26	78.691	66.13	1.402
Ag	0.11	3.11	0.33	1.25	0.08	0.49	0.04	0.91	0.092	0.088	11.344
Mo	0.97	0.52	0.51	1.24	0.95	0.56	0.34	1.22	1.137	0.78	1.533
As	17.39	2.08	36.14	2.24	13.15	0.64	8.41	1.70	11.091	7.75	5.683
W	4.26	4.93	21.03	2.73	2.76	0.45	1.24	1.77	1.64	1.56	26.18
Sb	1.33	6.62	8.82	2.25	0.92	0.6	0.55	1.56	1.176	0.59	23.182

Kk = Global Average element content/background value of West Qin Mountains area (Kk to eliminate before, Kk_0 for Elimination).
D: Superposed value = $\frac{\overline{X}}{\overline{X}_0} \cdot \frac{S}{S_0}$.

ore-forming potential. The elements with strong differentiation (C_v% = 50–75) are Mo and Cu, which are distributed unevenly in the strata and have some ore-forming potential. The concentration degree of each element can be divided into impoverishment and enrichment according to the values of concentration coefficient (KK) and superposition strength (*D*).

The Concentration Coefficient K & GT; 1.1 indicates that the elements are enriched in different degrees; the element superposition value $D \geq 2.0$ indicates that the elements have strong epigenetic superposition and the ore-forming possibility is high, while d = 1.2–2.0 indicates that the elements have strong superposition; it has a certain ore-forming ability. Enrichment elements: Au, Hg, Pb, Zn, Ag, Mo, As, Sb, and W, are obviously enriched in the area, and there is some mineralization, which is basically consistent with the metallogenetic elements in this area. Dilution element: Cu is a dilution element in the area, and the mineralization is relatively weak.

3.2 Feature extraction based on KPCA

In order to reduce the complexity of the retrieval model and improve the accuracy of the model, 10,756 geochemical data points were obtained from 1:50,000 river sediment measurements at known coordinates, and the corresponding geochemical data were located in the ESRI ArcGIS software; the resolution of all bands in the input remote sensing data is 30 m, and the image pixel value is the central one of the sampled pixels. Thus, there are 1,573 × 3,678 pixels in the preprocessed Landsat 8 OLI remote sensing image, and each pixel corresponds to 7 bands. Then, band ratio was used to enhance hydroxyl and iron corrosion information to suppress interference [15]. Finally, the KPCA model is used to reduce the dimension and correlation of the remote sensing data [16]. The steps of KPCA were implemented in Python as follows:

(1) By data = pd.read_excel(data) read the table data, X = data[data.columns[10:]] take a partial column in the table as an argument to X, y = data['Au'] dependent variable to y, Data Standardization X = StandardScaler ().fit_transform(X);
(2) Calculating the Kernel Matrix with gauss kernel function, k(i,j) = exp(−norm(x − y)^2/(2*sigma^2));
(3) Centralization Kernel Matrix, zero_k = k-zero_m*k-k*zero_m + zero_m*k*zero_m;
(4) Calculating eigenvalues and eigenvectors, data_v is eigenvector, data_e is eigenvalues, which is a diagonal, [data_v,data_e] = eig(zero_k); data_e = diag(data_e);
(5) The eigenvector matrix is sorted according to the eigenvalues, v = fliplr(data_v);
(6) Divide each row of v by the value of data for the corresponding row, v = v/sqrt(data_e());
(7) By zero_k*v, to get the principal component , data_all = zero_k*v.

3.3 Retrieval model based on ABC–SVM

In the research of remote sensing geochemistry inversion, scholars at home and abroad have used many methods to construct remote sensing geochemistry inversion model,

Table 3: Contribution to variance

	Component weight1	Component weight2	Component weight3	Component weight4	Component weight5	Component weight6
Explained_variance_ratio	0.9950000	0.0032500	0.0014100	0.0002580	0.0000370	0.0000195

Table 4: KPCA result matrix

X	*Y*	KPCA
104.8163479	34.68140427	0.563806984
104.622753	34.68015221	−0.383180087
104.9526398	34.68056282	−0.110681454
104.6216672	34.68003971	0.704978135
...	...	...
104.137078	34.34724924	−0.285454099
104.1764595	34.34732905	−0.366864367
104.2008568	34.34799774	0.143561125
104.2356612	34.34822817	0.727217185

but there are still two problems. First, in the process of feature extraction from remote sensing data, the traditional methods ignore the strong correlation and non-linearity among the bands of remote sensing data. The second is the limitation of the inversion model, because of the discontinuity of the abnormal distribution of the geochemistry and the nonlinear characteristics of the remote sensing data bands, the selection of the machine learning method is crucial, and the selected model should be able to fit this feature of the data well.

Both KPCA and ABC–SVM are used to establish the retrieval model, and it can be summarized as the following steps:

(1) Unify the coordinates of the geochemical data and the remote sensing data, and project the processed geochemical data with the coordinates to the remote sensing image map to obtain the element information; then, the feature values are extracted to reduce the dimension and remove the redundancy of the remote sensing data.
(2) Divide the dimension-reduced remote sensing data and geochemical data into training data and test data according to the 7:3 ratio.
(3) Using the ABC algorithm to obtain the optimal kernel parameters and penalty factors of SVM.
(4) Train the ABC-optimized SVM, and obtain the retrieval model based on the ABC–SVM.

Table 6: Evaluation results for Ag element

Regression model	EVS	MAE	MSE	R^2
Bayesian ridge	0.000001	0.796079	160.791724	0.000001
Linear regression	0.000457	0.827213	160.718487	0.000457
Elastic net	0.000000	0.796101	160.791908	0.000000
SVM	0.933765	0.659389	22.4849270	0.933765
ABC–SVM	0.983862	0.436333	2.59486900	0.983862

Table 7: Evaluation results for Hg element

Regression model	EVS	MAE	MSE	R^2
Bayesian ridge	0.009504	0.248174	0.142842	0.009504
Linear regression	0.009560	0.248248	0.142834	0.009560
Elastic net	0.000000	0.248797	0.244213	0.000000
SVM	0.868976	0.242790	0.145406	0.868976
ABC–SVM	0.937697	0.234674	0.122348	0.937697

4 Results and discussion

4.1 Feature extraction results

As shown in Table 3, the contribution rate of component 1 is over 99.5%, which indicates that the parameters are no

Table 5: Evaluation results for gold element

Regression model	EVS	MAE	MSE	R^2
Bayesian ridge	0.000000077	1.100819	156.030888	0.000000077
Linear regression	0.000119319	1.099570	156.012282	0.000119319
Elastic net	0.000000000	1.100830	156.030900	0.000000000
SVM	0.920879000	0.778839	12.3453180	0.920879000
ABC–SVM	0.991588953	0.504223	1.31238344	0.991588952

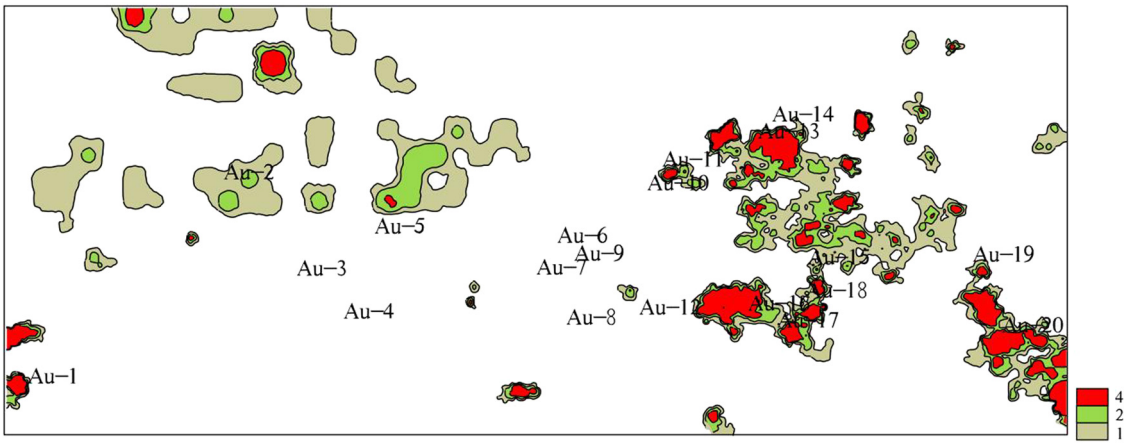

Figure 3: Distribution of gold anomalies based on the original geochemistry data.

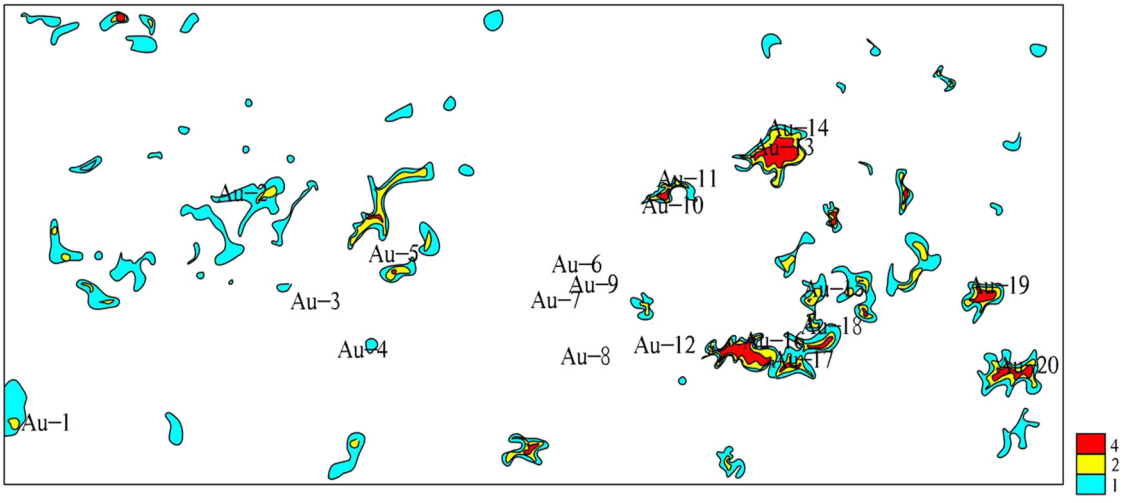

Figure 4: Distribution of gold anomalies based on the SVM-retrieved geochemistry data.

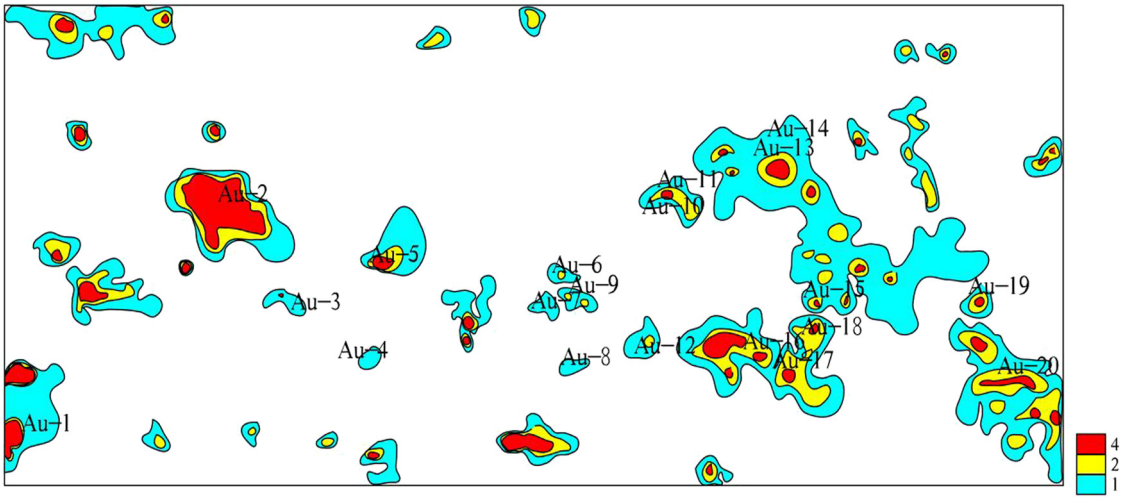

Figure 5: Distribution of gold anomalies based on the ABC–SVM-retrieved geochemistry data.

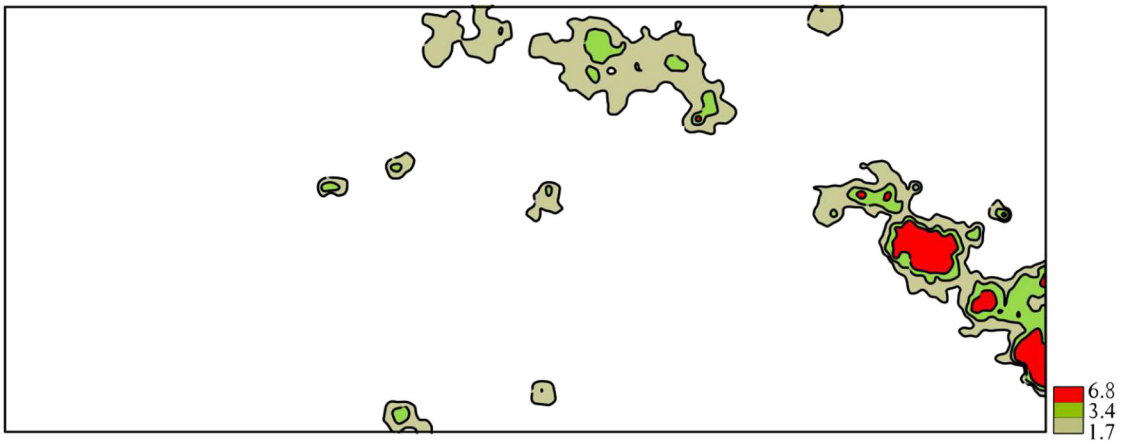

Figure 6: Distribution of silver anomalies based on the original geochemistry data.

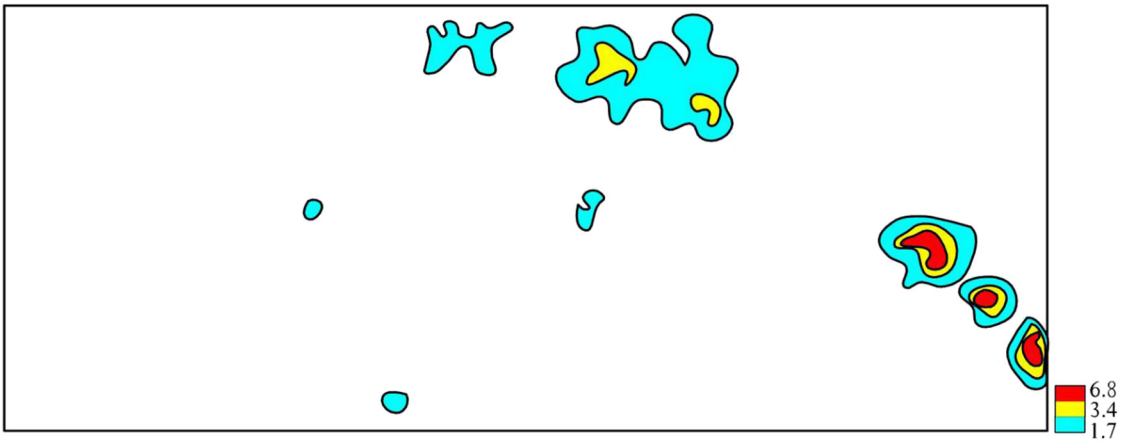

Figure 7: Distribution of silver anomalies based on the SVM-retrieved geochemistry data.

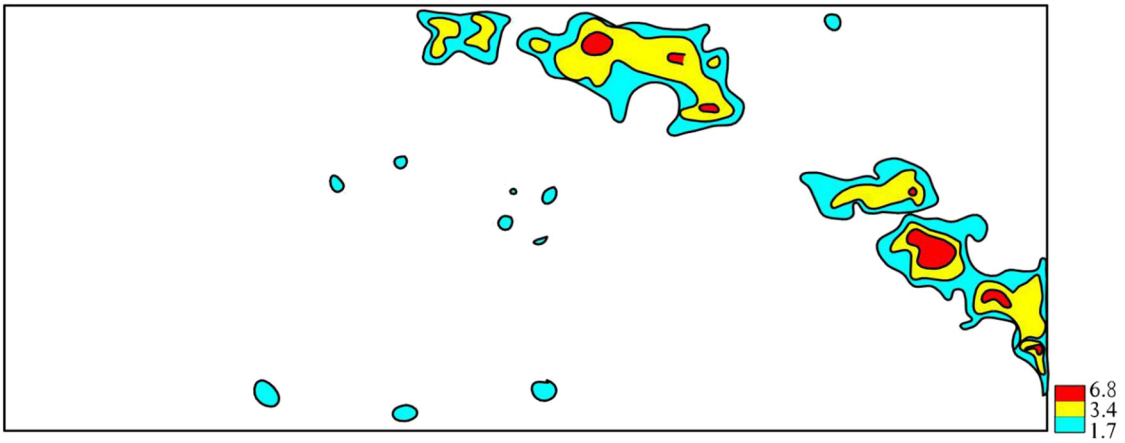

Figure 8: Distribution of silver anomalies based on the ABC–SVM-retrieved geochemistry data.

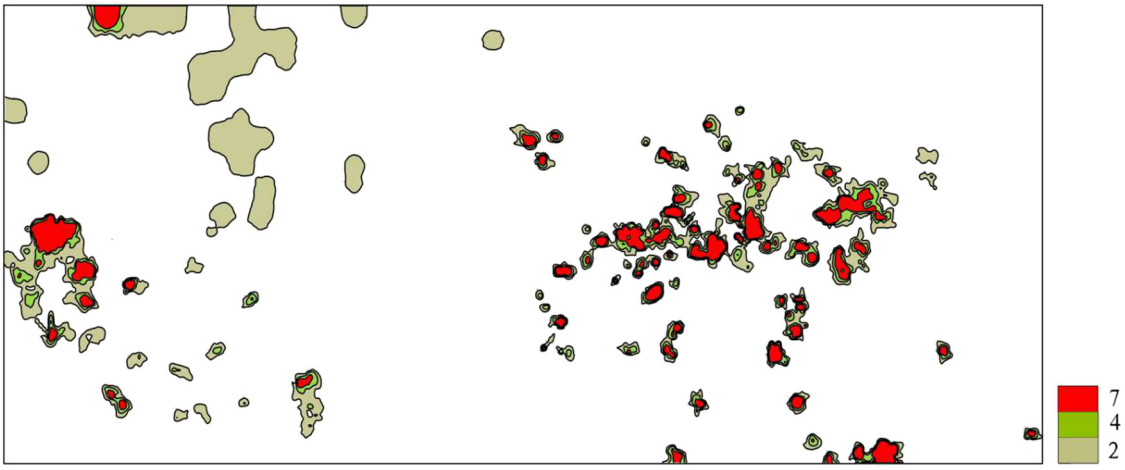

Figure 9: Distribution of mercury anomalies based on the original geochemistry data.

longer adjusted since they are best in the parameters. The first principal component is shown in Table 4, and X and Y represent the corresponding coordinates.

4.2 Retrieval results

The study area is the Zhaishang–Mawu area in Gansu Province, and the main mineral in the area is gold. Therefore, based on the collected geochemistry data, the gold elements with known ore spots were selected for experimental verification, and at the same time, the silver and mercury data were used to delineate the anomalies. The specific steps are as follows: First, the area of Remote Sensing Data Grid Division choose 300 × 300 m division, Grid Center data as the block of data, access to data 37,500. The dimensionality is reduced by KPCA, and the reduced data are input as an independent variable into the established model.

In order to verify the validity of the model, Bayesian Ridge Regression Model, Linear Regression Model, Elastic Network Regression Model, and SVM and ABC–SVM are established, respectively. The effects of different models are evaluated by gold, silver, and mercury, and the results of the comparison are shown in Tables 5–7 (Variance Score (EVS), between 0 and 1, and the larger is the better for fit; The Mean Absolute Error (MAE), the approximation of the calculated model results to the actual results, and the smaller is the better; Mean Square Error (MSE), and the smaller is better; R^2: Judging Coefficient, between 0 and 1, and the larger behalf of the better). As can be shown from the tables, the ABC–SVM has better results than other models.

4.2.1 Results of Aurum

Furthermore, in order to examine the results of SVM and ABC–SVM models with the gold anomalies circled by the original geochemistry data, 20 known mineralization sites

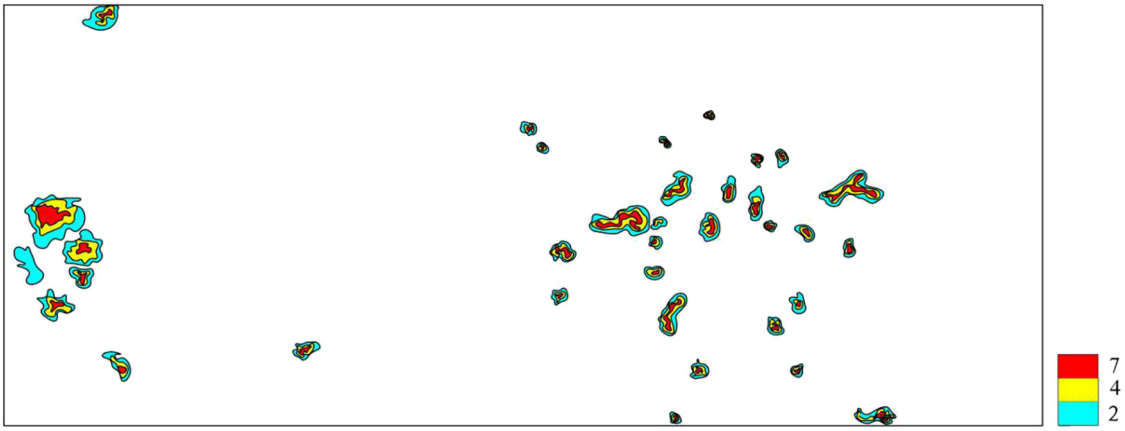

Figure 10: Distribution of mercury anomalies based on the SVM-retrieved geochemistry data.

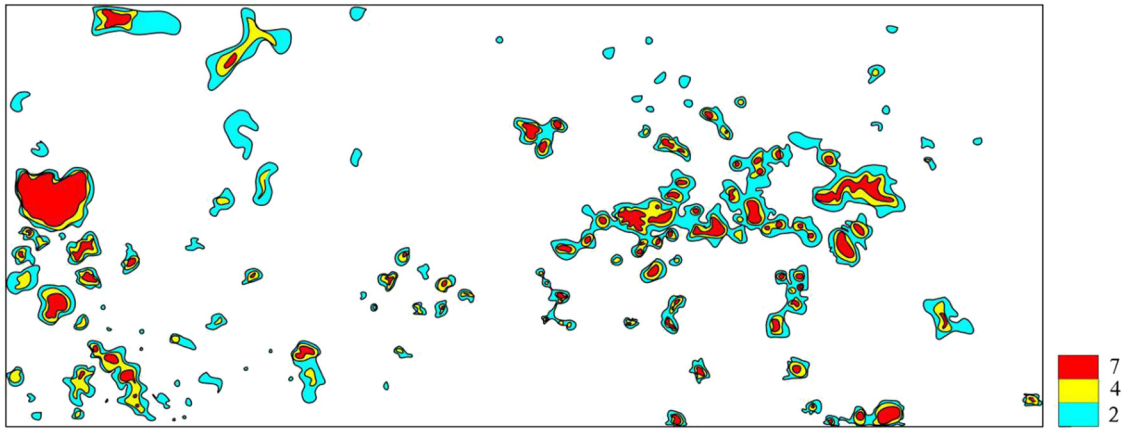

Figure 11: Distribution of mercury anomalies based on the ABC–SVM-retrieved geochemistry data.

are compared. Figures 3–5 show respectively the distribution of the golden anomalies delineated by the original geochemistry data, the anomalies delineated by the results of the SVM retrieval model, and the anomalies delineated by the results of the ABC–SVM retrieval model. The abnormity lower limit is calculated according to $T = +2\delta$, the iso-content line is drawn according to the 1, 2, and 4 times of the abnormity lower limit value, and the three concentration zones are divided into the outer, middle, and inner bands of the anomalies with blue, yellow, and red, respectively. It is obvious that the anomaly distribution retrieved from the ABC–SVM model is more consistent with the original geochemistry data than that delineated by the SVM model.

4.2.2 Results of Argentum

Figures 6–8 show the distributions of the silver anomalies delineated from the original geochemistry data, the anomalies delineated from the results of the SVM retrieval model, and from ABC–SVM retrieval model, respectively. The abnormity lower limit is calculated according to $T = +2\delta$, the iso-content line is drawn according to the 1.7, 3.4 and 6.8 times of the abnormity lower limit value, and the three concentration zones are divided into the outer, middle, and inner bands of the anomalies with blue, yellow, and red, respectively. It is obvious that the anomaly distribution retrieved from the ABC–SVM model is more consistent with the original geochemistry data than that delineated by the SVM model.

4.2.3 Results of hydrargyrum

Figures 9–11 are the distributions of the mercury anomalies delineated from the original geochemistry data, the anomalies delineated from the SVM model, and the anomalies delineated from the ABC–SVM model, respectively. The abnormity lower limit is calculated according to $T = +2\delta$, the iso-content line is drawn according to the 2, 4, and 7 times of the abnormity lower limit value, and the three concentration zones are divided into the outer, middle, and inner bands of the anomalies with blue, yellow, and red, respectively. It is obvious that the anomaly distribution retrieved from the ABC–SVM model is more consistent with the original geochemistry data than that delineated by the SVM model.

5 Concluding remarks

The main conclusions and innovations of this research work are reflected in the following two points: (1) The KPCA method can solve the problem of remote sensing data presenting strong correlation and nonlinear characteristics due to the large amount of data and excessive redundant data. (2) SVM uses inner product kernel functions to map to high-dimensional space, with good generalization ability and robustness, but the choice of parameters can have a large impact on its performance. The ABC, through the simulation of bee colony honey harvesting activities, solves high-dimensional problems and multi-objective optimization problems; the algorithm is an efficient and good solution, combining ABC with SVM; the inverse model performance is better. However, this retrieval model does not take into account more geologic information of the study area; it should be considered in future research work.

Acknowledgments: This research work was supported by the National Key Research and Development Program of China (No. 2020YFA0714103), China Scholarship Council

(No. CSC201906175002), and the Young Teachers and Students' Cutting-edge Funding of Jilin University, China (No. 2022-JCXK-31). We also thank the anonymous reviewers for their helpful suggestions.

Author contributions: Writing the original draft, Jinxin He; writing review and editing, Debo Chen; supervision and made improvements to the manuscript, Ye Zhan; collecting data and data processing, Xiaoyu Ren; data processing, Qingyi Li.

Conflict of interest: Authors state no conflict of interest.

References

[1] Pieters CM, Englert PA. Remote Geochemical Analysis: Elemental and Mineralogical Composition[M]. New York: Cambridge University Press; 1993.
[2] Wu Y, Tian Q, Ji J, Chen J. Study on the remote-sensing geochemistry. Adv Earth Sci. 2003;18(2):228–35 (in Chinese).
[3] Swayze GA. The Hydrothermal and Structural History of the Cuprite Mining District,Southwestern Nevada: An Integrated Geological and Geophysical Approach[D]. Colorado: University of Colorado; 1997.
[4] Fojun Y, Jianmin Y, Hongqi C, Tianping Z, Yubin L, Chaoqiang L, et al. A remote sensing Cu geochemical model for the Duolong ore concentration area. Tibet Acta Petrologica et Mineralogica. 2015;34(5):710–20 (in Chinese).
[5] Aronoff S, Goodfellow W. Image processing for the effective analysis of regional geochemical data. Canada; 1985.
[6] Eliason PT, Donovan TJ, Chavez PS. Integration of geologic, geochemical, and geophysical data of the cement oil field, oklahoma, using spatial array processing. Seg Technical Program Expanded Abstr. 1982;1(1):474–5.
[7] Zhang X. Coupling stdudy of remote sensing alteration anomalies and geochemical anomaly in copper polymetallic ore district – Take derong binchuan area as an example[D]. Chengdu University of Technology; 2016 (in Chinese).
[8] Zhao H. Research on a remote-sensing geochemistry nonlinear inversion model based on ETM + data in Lalingzaohuo region[D]. Jilin University; 2017 (in Chinese).
[9] Pan C. Study on the hyperspectral remote sensing inversion of soil heavy metal concentrations based on random forest model[D]. China University of Mining and Technology; 2017 (in Chinese).
[10] Ren Q, Li M, Han S. Discrimination and comparison experiments of basalt tectonic setting based on improved genetic algorithm – optimized neural network. Earth Sci Front. 2019;26(04):117–24 (in Chinese).
[11] Li S, Li L, Milliken R, Song K. Hybridization of partial least squares and neural network models for quantifying lunar surface minerals. Icarus. 2012;221(1):208–25.
[12] Bachri I, Hakdaoui M, Raji M, Teodoro AC, Benbouziane A. Machine learning algorithms for automatic lithological mapping using remote sensing data: A case study from souk arbaa sahel, sidi ifni inlier, Western Anti-Atlas, Morocco. Int J Geo-Information. 2019;8(6):248.
[13] Yunkai G, Jia Q, Ming J, Qiong Z. Hyper-spectral inversion of cu content in mining soil based on kernels partial least-squares. Chin J Soil Sci. 2019;50(1):52–6 (in Chinese).
[14] Chengzhao LI, Shuai HA, Mingchao LI, Yueqin ZH. Prediction and analysis of gold deposit sizes based on coupled PCA–SVM algorithm. Earth Sci Front. 2019;26(4):138–45.
[15] Yiquan W, Donghui S, Yang Z. Remote sensing mineralization alteration information extraction based on PCA and SVM optimized by cuckoo algorithm. J Remote Sens. 2018;22(5):810–21 (in Chinese).
[16] Youjing Z, Hao H, Xuemei M. Research on classification for city's vegetation type based on KPCA and SAM. Geogr Geo-Information Sci. 2006;(3):35–8 (in Chinese).